Annual Progress Report,

covering the period

1 June 1973 to 31 August 1974

for

GRANT NGR 05017027

entitled

STUDIES IN MATTER ANTIMATTER SEPARATION AND IN THE ORIGIN OF LUNAR MAGNETISM

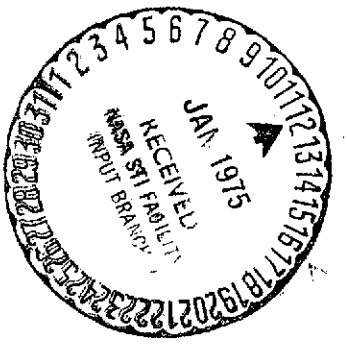

conducted by

William A. Barker, Principal Investigator

Ronald Greeley, Curtis Parkin, and Hans Aggarwal,
Coinvestigators

University of Santa Clara
California 95053

The NASA Technical Officer for this grant is
Dr. I. Poppoff, Space Sciences Division,
Ames Research Center, NASA, Moffett Field, CA. 94035

TABLE OF CONTENTS

I. Introduction

This report summarizes the results of research performed on the subject grant from approximately 1 June 1973 to 31 August 1974. The research was conducted by the Principal Investigator and three Research Associates and the results are presented in four parts, one for each investigator.

Annual Progress Report

William A. Barker
Department of Physics
University of Santa Clara
Santa Clara, CA 95053

I. Introduction

The ambiplasma is a mixture of ordinary (koino) matter and antimatter. Its properties are of interest in connection with the as yet undetermined role which antimatter plays in cosmology.

Relativistic quantum mechanics (Dirac, 1930 and 1947; Streater and Wightman, 1964) requires that antimatter exist. Evidence from elementary particle physics supporting this requirement is abundant. Corresponding to the familiar particles of ordinary matter–the electron, the proton, the neutron, the neutrino, etc., there exist antiparticles–the positron, the antiproton, the antineutron, the antineutrino, etc. Although all of the elementary particles do seem to have antiparticles, not all are distinguishable from their particle counterparts. Thus the photon and the antiphoton are indistinguishable as are the π° and $\bar{\pi}^\circ$. Such pairs are called self conjugate.

In astrophysics the significance of antimatter is well established. The luminosity of the sun and of the stars depends on fusion processes like

$$p + p \rightarrow d + \bar{e} + \nu_e \qquad (1)$$

in which antimatter, in the form of positronium, is generated. However, the mean free pair-annihilation path of a positron in a stellar interior is so short that its direct detection is not feasable.

The detection of large quantities of antimatter in the universe is made difficult by the fact that there is such complete elementary particle symmetry. Atoms and antiatoms formed from these particles

are not readily distinguishable. Thus the radiation from an antihydrogen atom, consisting of an antiproton and a positron, is the same as from a hydrogen atom. Zeeman or Stark effects in anti-atoms are only distinguishable from these effects in atoms if the direction of the magnetic or electric field is known. In principle one can assert that every other star or every other galaxy is made of antimatter.

If the Andromeda galaxy were primarily antimatter, then anti-neutrinos from the reaction

$$\bar{p} + \bar{p} \rightarrow \bar{d} + e + \bar{\nu}_e \qquad (2)$$

would induce the formation of antileptons in detection systems on the earth. However the state of the art in neutrino astronomy precludes such a measurement.

A mixture of matter and antimatter generates annihilation radiation. Electrons and positrons annihilate into two gammas each of energy 0.511 Mev. Nucleon anti-nucleon pairs annihilate into pions. Of these the neutral pions produce gammas which peak in energy around 70 Mev. These higher energy gammas are more readily detectable. A review of the gamma ray observations (Steigman, 1969) sets upper limits on admixed annihilating antimatter at $3 \times 10^{-6}\ M_\odot$ in the galactic center, at $10^{-5}\ M_\odot$ in interstellar gas and at $n_- \lesssim 4 \times 10^{-12}\ cm^{-3}$ in intergalactic gas, if the universe is closed.

It has been suggested (Vlasov, 1965; Barker et al., 1966) that an ambiplasma consisting of electrons and positrons could, under suitable conditions, form the atom positronium, whose radiation from the galactic center might be detectable. We investigate this question more carefully in Section II of this paper.

II. Detection of Positronium at the Galactic Center

What physical conditions must prevail at the center of the galaxy in order that spectral lines from the atom positronium can

be observed by ground based instruments?

We consider two criteria. The positronium line must be of sufficient intensity at any one time so that it is detectable. This intensity should persevere over a period of $\sim 10^{+10}$ years rather than exist as a transient phenomenon which could be observed only as a matter of accident at any one time.

We focus our attention on the Paschen alpha ($4 \rightarrow 3$) transition in positronium. The wavelength of this radiation is 3.75 microns. At this wavelength the earth's atmosphere is transparent. It is possible in a 10-second integration time to detect a near infrared line whose power is 10^{-15} watts. The lower limit of observability with the present state of the art can probably be extended to 10^{-17} watts. (Augason, 1974)

Consider a detector whose collector area is denoted by A_c at a distance R from a source whose luminosity is L_{min}. Then

$$L_{min} = \frac{4\pi R^2}{A_c} P_D \qquad (3)$$

where P_D represents the detectable power at the collector. The distance to the galactic center $R = 8.2 \times 10^3$ parsecs $= 2.52 \times 10^{20}$ meters. A typical collector area $A_c = 4 \times 10^{-1}$ meters. From Eq. (3), we find that $L_{min} = 2.02 \times 10^{32}$ ergs/sec for $P_D = 10^{-17}$ watts.

The luminosity of positronium Paschen-alpha radiation at the galactic center

$$L_c = -h\nu \frac{dN}{dt} \qquad (4)$$

where N is the number of positronium atoms undergoing the $4 \rightarrow 3$ transition with an energy release $h\nu = 5.3 \times 10^{-13}$ ergs. We assume that positronium atoms are being formed by the radiative capture of electrons and positrons which we consider to be uniformly distributed over a sphere of radius r = 700 parsecs, which is a reasonable value for the radius of the galactic center (Woltjer, 1965). It has been shown that this capture occurs primarily in the high angular momentum states (Bates et al, 1939). Inasmuch as radiative transitions occur at the fastest rates for $\Delta\ell = \pm 1$ and

the largest possible jumps in principal quantum number, it is highly probable that most of the positronium atoms formed cascade down to the n = 4 state and then emit the Paschen, Balmer and Lyman alpha photons before undergoing annihilation. This latter process is slow compared to the radiative process described for all states except the S states of positronium. Hence we may write

$$\frac{dN}{dt} = \frac{4}{3}\pi R^3 \frac{dn}{dt} \tag{5}$$

where n = the electron positron number density and

$$\frac{dn}{dt} = -\frac{n^2 \sigma_{re} v}{2} \tag{6}$$

where σ_{re} is the radiative capture annihilation cross section (Morgan and Hughes, 1970) for electrons and positrons with a relative velocity v. Integrating Eq. (6) yields

$$n = \frac{n_0}{1 + \frac{t}{2} n_0 v \sigma_{re} t} \tag{7}$$

where n_0 is the initial electron-positron number density. If we take t to be the age of the universe $\tau_0 = 3.16 \times 10^{17}$ seconds, then the present positronium Paschen alpha luminosity at the galactic center

$$L_c = \frac{\frac{4}{3}\pi R^3 n_0^2 \sigma_{re} v h\nu}{\left(1 + \frac{1}{2} n_0 \sigma_{re} v \tau_0\right)^2} . \tag{8}$$

The most optimistic value for L_c occurs for n_0 infinite.

$$\lim_{n_0 \to \infty} L_c = \frac{16\pi R^3 h\nu}{3 \sigma_{re} v \tau_0^2} \tag{9}$$

The condition for the observability of positronium under these favorable assumptions then becomes

$$\sigma_{re} v \leq \frac{16\pi R^3 h\nu}{3 L_{min} \tau_0^2} = 4.41 \times 10^{-15} \text{ cm}^3 \text{ sec}^{-1} \tag{10}$$

The left hand side of the inequality (10) is a function of kinetic energy in the center of mass frame and can be obtained from the literature (Morgan and Hughes, 1970). In Table 1, values of $\sigma_{re} v$ are given for four different energies. The most favorable energy is 50 ev which yields a $\sigma_{re} v$ which is an order of magnitude larger than required for detectability.

K_e (ev)		v (cm/sec)	v (cm^3/sec)
50	72.5	5.94×10^8	1.06×10^{-14}
10	7.25×10^3	2.66×10^8	4.72×10^{-13}
1	4.73×10^4	8.40×10^7	8.99×10^{-13}
.05	1.29×10^6	1.88×10^7	5.94×10^{-12}

Table 1

Annihilation cross sections as a function of energy.
$\sigma_o = 2.5 \times 10^{-25}$ cm^2.

Energies higher than 50 ev are not considered because above this energy electrons and positrons have a greater probability of direct annihilation in flight than of forming positronium prior to annihilation.

We conclude that infrared radiation from positronium is not detectable from the center of the galaxy at the present time.

Annual Progress Report

Ronald Greeley
Department of Physics
University of Santa Clara
Santa Clara, CA 95053

I. Introduction

This report deals with research conducted on planetary geological processes by the investigator represented on the grant for 90% of his effort. Specific research topics include: 1) terrestrial field studies of volcanic terrain in Idaho and Hawaii, 2) laboratory simulations of aeolian processes, 3) interpretation of volcanic features on the Moon and Mars, and of aeolian features on Mars, and 4) application of infrared line-scanning imagery to terrestrial geological problems.

II. Summary of Research

Results of this research were published in journals or presented orally at meetings. Published abstracts from these journals and meetings are as follows:

Science, v. 183, (1974)

Wind Tunnel Simulations of Light and Dark Streaks on Mars

Ronald Greeley
J. Iversen, J. Pollack, N. Udovich, and B. White

ABSTRACT

Wind tunnel experiments have revealed a characteristic flow field pattern over raised-rim craters which causes distinctive zones of aeolian erosion and deposition. Comparisons of the results with Mariner 9 images of Mars show that some crater-associated dark zones result from wind erosion and that some crater-associated light streaks are depositional.

NASA TM X-62, 343, 1974 and in press Proc.
Remote Sensing Symposium

Use of Visible, Near-Infrared, and Thermal Infrared Remote Sensing to Study Soil Moisture

Maxwell B. Blanchard
Ames Research Center, NASA, Moffett Field, California 94035

Ronald Greeley
University of Santa Clara, Santa Clara, CA 95053

and

Robert Goettelman
LFE Corporation, Richmond, California 94804

ABSTRACT

Measuring soil moisture remotely is an objective for many investigators. Applications of remotely determined soil moisture range from agriculture (where moisture relates to crop growth) to civil works (where moisture relates to slope failures in levees, dams, and along highways). Two methods are used to estimate soil moisture remotely using the 0.4- to 14.0-micron wavelength region: (1) measurement of spectral reflectance, and (2) measurement of soil temperature. The reflectance method is based on observations which show that directional reflectance decreases as soil moisture increases for a given material. The soil temperature method is based on observations which show that differences between daytime and nighttime soil temperatures decrease as moisture content increases for a given material. In some circumstances, separate reflectance or temperature measurements yield ambiguous data, in which case these two methods may be combined to obtain a valid soil moisture determination. In this combined approach, reflectance is used to estimate low moisture levels; and thermal inertia (or thermal diffusivity) is used to estimate higher levels. The reflectance method appears promising for surface estimates of soil moisture, whereas the temperature method appears promising for estimates of near-subsurface (0 to 10 cm). Both methods require additional laboratory and field investigations.

In press. European Geophysical Union, 1974 Annual Meeting
Trieste, Italy

Analysis of MARTIAN AEOLIAN PROCESSES

Ronald Greeley
NASA-Ames Research Center, Moffett Field, CA 94035
University of Santa Clara, Santa Clara, CA 95053

J. Iversen
Iowa State University, Ames, Iowa 50010

J. Pollack
NASA-Ames Research Center, Moffett Field, CA 94035

Recent Mariner 9 spacecraft results for Mars show that aeolian processes are significant in the geological modification of the martian surface. Wind tunnel simulations conducted at NASA-Ames and Iowa State University provide insight to the complex martian aeolian environment. Threshold speed studies indicate that near-surface wind speeds on Mars in excess of 300 km/hr are required to initiate motion of optimum-size grains on flat terrain. Threshold speed is influenced in part by surface roughness; extrapolation of wind tunnel results to Mars shows that the change in surface roughness from smooth plains to the blocky ejecta around impact craters could result in differential erosion to produce pedestal craters. Modeling experiments of flow over craters show distinctive patterns of erosion and deposition, indicating that some martian crater dark streaks are erosional and some light streaks are depositional. An erosion-rate parameter experimentally derived was applied to the Daedalia region using Mariner 9 results and to a first approximation, we estimate that about 0.4 to 2.4 mm of aeolian material was eroded from the wake of some craters during a 38 day period of the mission. Other modeling experiments support the hypothesis (Veverka et al., MS) that the large crater-associated dark plume in Cerberus could be of internal (possibly volcanic) origin. Future work includes refinement of Mariner 9 data, initiation of low pressure wind tunnel experiments, and comparisons of results with various terrestrial analogs.

Trans. Amer. Geophy. Union
V. 54, No. 11 (1973)

Laboratory Simulations of Wind Erosion and Deposition Associated with Martian Craters

Ronald Greeley
Dept. of Physics, Univ. of Santa Clara, Santa Clara, CA 95053

J. B. Pollack
Space Science Division, NASA-Ames Res. Ctr., Moffett Field, CA 95035

J. D. Iversen
Dept. Aerospace Engineering, Iowa State Univ., Ames, Iowa 50010

Mariner 9 images of Mars show many craters with light and dark surface streaks interpreted to be aeolian in origin. A series of wind tunnel experiments has been conducted to determine the aerodynamic flow field over craters and to assess the zones of relative aeolian erosion and deposition associated with raised-rim craters. Preliminary results indicate that a horseshoe vortex wraps around the crater rim and forms two trailing vortices in the crater wake, resulting in a distinctive bilobate erosional pattern (zones of high surface stress) and trilobate depositional pattern. While this general pattern of erosion and deposition appears to be constant for raised-rim craters, the exact size, shape, and position of the zones is dependent, at least in part, on the crater geometry, wind speed, and time. Comparisons of results with martian analogs indicate that some crater-associated dark streaks are zones that have been swept free of surface particles, and that some crater-associated light streaks are aeolian deposits.

Trans. Amer. Geophys. Union
V. 54. No. 11 (1973)

Split Butte Crater (Idaho) and its Planetological Implications

John S. King
Dept. Geol. Sciences, State Univ. New York, Buffalo, New York 14207

Ronald Greeley
Dept. of Physics, Univ. of Santa Clara, Santa Clara, CA 95053

The crater, which is on the central Snake River Plain, displays morphological characteristics that should be useful in the interpretation of planetary surface features. It is a distinct raised-rim crater standing well above the basaltic plain and consists of an outer discontinuous tephra ring 600 m in diameter and an inner ovoid collapse pit crater 420 m in diameter, thus giving the appearance of a concentric impact crater. The outer flanks of the crater have been encroached by younger basalt flows, accounting for the ringed, moat-like depression surrounding the crater.

The outer asymmetric tephra ring is well layered and dips away from the central depression. Its asymmetry appears to have resulted from the prevailing wind at the time of deposition as well as subsequent preferential erosion. The inner part of the crater is layered basalt that was apparently a lava lake contained by the trephra ring. The central part of the lake collapsed, forming the present inner pit crater. Detailed petrographic, structural, and geomorphic analyses are currently in progress. Split Butte is one of three possibly similar structures on the Plain which appear to be unique. The other craters, Sand Butte and China Cap, are being studied to determine their differences and similarities to Split Butte.

Geol. Soc. Amer. V. 6, No. 3 (1974)

USE OF THERMAL INFRARED IMAGERY IN LANDSLIDE ANALYSIS AND THE POTENTIAL FOR REMOTELY MONITORING MASS MOVEMENT

Ronald Greeley
University of Santa Clara, Santa Clara, CA 95053

M. B. Blanchard
NASA-Ames Research Center, Moffett Field, CA 94035

R. H. Gelnett
U.S.A. Corps of Engineers, San Francisco, CA 94102

Water in unconsolidated sediments is one of the primary causative factors leading to landslides. Rapid increase in water content is often the triggering mechanism is disastrous landslides. Thus, the ability to determine the moisture content of sediments for known conditions of slope, structure, etc., would permit evaluation of specific areas in terms of the potential for mass movement. Currently, such analyses are possible only from ground studies of limited areas because there is no developed technique for determining remotely the moisture content of sediments. However, preliminary studies have shown that it is possible to correlate soil temperature with soil moisture. Changes in soil surface temperature can be monitored remotely by employing airborne infrared imagers. Typically, these instruments are capable of detecting temperature differences of ± 0.2°C for areas on the ground a few square feet in size. Initial studies obtained over selected landslides in the San Francisco Bay Area indicate landslides are well defined on thermal infrared imagery and specific zones of active water seepage can be identified. If further studies can be quantified, then it may be possible to monitor from airborne platforms large areas for potential landslides.

Geol. Soc. Am. V. 6, No. 5 (1974)

APPLICATIONS OF THERMAL INFRARED IMAGERY TO HIGHWAY PROBLEMS

Ronald Greeley
University of Santa Clara, Santa Clara, CA 95053

M.B. Blanchard
NASA-Ames Research Center, Moffett Field, CA 94035

H. Shade
NASA-Ames Research Center, Moffett Field, CA 94035

E. Eagle
Division of Highways, State of California

Concrete highways often have buried defects that are difficult or impossible to detect. Such defects include voids, inhomogeneities (pockets of aggregate, soil, etc.), and reinforcing rods that have shifted. At present, these defects are found by random drilling, a process that is expensive because of the number of holes involved, and which often misses small but potentially critical defects. Because these buried defects have different thermal properties than concrete, it should be possible to locate them by employing thermal infrared imagery to locate surface temperature anomalies. To test this hypothesis, concrete test slabs (some containing defects) were studied using an infrared imager. Preliminary results showed that some subsurface defects (voids in this case) were easily located. A second problem involves asphalt highways under which surface water runoff, or groundwater, may flow. When this occurs, the asphalt deteriorates rapidly. Unfortunately, it is seldom possible to determine when and where this occurs without detailed investigations to locate the source and flow of the water beneath the asphalt. However, these zones should show as thermal anomalies on asphalt roadways because the thermal properties of the dry soil beneath the road are different than those of the wet soil. Preliminary tests have shown

that it is possible to define some moisture-laden zones beneath test samples of asphalt roadway. Future work involves additional experiments to determine the limits of detection under field conditions.

Annual Progress Report

Curtis Parkin
Department of Physics
University of Santa Clara
Santa Clara, CA 95053

I. Introduction

Magnetometers were set up at four Apollo sites on the surface of the moon during the time period November 1969 to April 1972 as part of a geophysical experiments package. The purpose of the magnetometer experiments has been to measure remanent and induced lunar magnetic fields in order to investigate the following properties of the lunar interior and lunar environment: (1) lunar electrical conductivity and temperature, (2) lunar magnetic permeability and iron abundance, (3) lunar remanent magnetic fields and their interaction with the solar wind plasma, and (4) properties of the earth's magnetosphere. Results for the year ending August 31, 1974 have been reported in the publications and verbal presentations which are listed in section II and for which abstracts are included in section III.

II. List of Publications and Verbal Presentations

A. Publications

1. Parkin, C. W., Dyal, P., and Daily, W. D., "Iron Abundance in the Moon from Magnetometer Experiments," Proc. Fourth Lunar Sci. Conf., Geochim. Cosmochim. Acta, Suppl. 4 (W. A. Gose, ed.), vol. 3, Pergamon Press, New York, pp. 2947-61, 1973.

2. Dyal, P., Parkin, C. W., and Daily, W. D., "Surface Magnetometer Experiments: Internal Lunar Properties," Proc. Fourth Lunar Sci. Conf., Geochim. Cosmochim. Acta, Suppl. 4 (W. A. Gose, ed.) vol. 3, Pergamon Press, New York, pp. 2925-45, 1973.

3. Dyal, P., and Parkin, C. W., "Global Electromagnetic Induction in the Moon and Planets," Phys. Earth Planet. Interiors 7, 251-65, 1973.

4. Dyal P., Parkin C. W., and Daily W. D., "Temperature and Electrical Conductivity of the Lunar Interior from Magnetic Transient Measurements in the Geomagnetic Tail," Proc. Fifth Lunar Sci. Conf., Geochim. Cosmochim. Acta, in press, 1974.

5. Parkin, C. W., Daily, W. D., and Dyal, P., "Iron Abundance and Magnetic Permeability of the Moon," Proc. Fifth Lunar Sci. Conf., Geochim. Cosmochim. Acta, in press, 1974.

6. Dyal, P., Parkin, C. W., and Daily, W. D., "Magnetism and the Interior of the Moon," Rev. Geophys. Space Phys., in press, 1974.

7. Dyal, P., Parkin, C.W., and Daily, W. D., "Lunar Electrical Conductivity, Permeability, and Temperature from Apollo Magnetometer Experiments," submitted to Proceedings of the Conference on Cosmochemistry of the moon and planets, Moscow, USSR, June 1974.

B. Verbal Presentations

1. Parkin, C. W., Dyal, P., and Daily, W. D., "Lunar Properties from the Apollo Surface Magnetometer Experiments," Second General Scientific Assembly, International Association of Geomagnetism and Aeronomy, Kyoto, Japan, 9-21 September 1973.

2. Kuckes, A. F., Beckwith, S. V., Daily, W. D., Dyal, P., and Parkin, C. W., "Lunar Electrical Conductivity Profile Analysis," Second General Scientific Assembly, International Association of Geomagnetism and Aeronomy, Kyoto, Japan, 9-21 September 1973.

3. Dyal, P., Parkin, C. W., and Daily, W. D., "Lunar Properties from the Apollo Surface Magnetometer Experiments," Geological Society of America Annual Meeting, Dallas, Texas, 12-14 November 1973.

4. Parkin, C. W., Daily, W. D., and Dyal, P., "Lunar Iron Abundance from Magnetometer Measurements," in Lunar Science V, p. 589, Fifth Lunar Science Conference, Houston, Texas, March 1974.

5. Dyal, P., Parkin, C. W., and Daily, W. D., "Global Lunar Properties from Magnetometer Measurements," in Lunar Science V, p. 193, Fifth Lunar Science Conference, Houston, Texas, March 1974.

6. Kuckes, A. F., Daily, W. D., Dyal, P., and Parkin, C. W., "Temperature Profile of the Lunar Interior," Trans. Amer. Geophys. Union (EOS), 55, p. 331, April 1974.

7. Daily, W. D., Dyal, P., and Parkin, C. W., "Magnetopause Velocity and Thickness Determined from a Network of Apollo Magnetometers," Trans, Amer. Geophys. Union (EOS), 55, p. 390, April 1974.

8. Dyal, P., Parkin, C. W., and Daily, W. D., "Electrical Conductivity, Permeability, and Temperature from Apollo Magnetometer Experiments," Conference on Cosmochemistry of the moon and planets, Moscow, USSR, June 1974.

III. Abstracts of Publications and Verbal Presentations:

Proceedings of the Fourth Lunar Science Conference
(Supplement 4, Geochimica et Cosmochimica Acta)
Vol. 3, pp. 2947-2961

Iron Abundance in the moon from magnetometer measurements

Curtis W. Parkin
Dept. of Physics, Univ. of Santa Clara, Santa Clara, CA 95053

Palmer Dyal and William D. Daily
NASA-Ames Research Center, Moffett Field, CA 94035

Abstract—Apollo 12 and 15 lunar surface magnetometer data with simultaneous lunar orbiting Explorer 35 data are used to plot hysteresis curves for the whole moon. From these curves a whole-moon permeability $\mu = 1.029^{+0.024}_{-0.019}$ is calculated. This result implies that the moon is not composed entirely of paramagnetic material, but that ferromagnetic material such as free iron exists in sufficient amounts to dominate the bulk lunar susceptibility. From the magnetic data the ferromagnetic free iron abundance is calculated. Then for assumed compositional models of the moon the additional paramagnetic iron is determined, yielding total lunar iron content. The calculated abundances are as follows: ferromagnetic free iron, 5±4 wt.%; total iron in the moon, 9±4 wt.%.

Proceedings of the Fourth Lunar Science Conference
(Supplement 4, Geochimica et Cosmochimica Acta)
Vol. 3, pp. 2925-2945

Surface magnetometer experiments: Internal lunar properties

Palmer Dyal
NASA-Ames Research Center, Moffett Field, California 94035

Curtis W. Parkin
University of Santa Clara, Santa Clara, California 95053

William D. Daily
NASA-Ames Research Center, Moffett Field, California 94035

Abstract—Magnetic fields have been measured on the lunar surface at the Apollo 12, 14, 15, and 16 landing sites. The remanent field values at these sites are respectively 38γ , 103γ (maximum), 3γ , and 327γ (maximum). Simultaneous magnetic field and solar plasma pressure measurements show that the remanent fields at the Apollo 12 and 16 sites are compressed and that the scale size of the Apollo 16 remanent field is $5 \leq L < 100$km. The global eddy current fields, induced by magnetic step transients in the solar wind, have been analyzed to calculate an electrical conductivity profile. From nightside data it has been found that deeper than 170 km into the moon, the conductivity rises from 3×10^{-4} mhos/m to 10^{-2} mhos/m at 1000 km depth. Analysis of dayside transient data using a spherically symmetric two-layer model yields a homogeneous conducting core of radius 0.9 R_{moon} and conductivity $\sigma = 10^{-3}$ mhos/m, surrounded by a nonconducting shell of thickness 0.1 R_{moon}. This result is in agreement with the conductivity profile determined from nightside data. The conductivity profile is used to calculate the temperature for an assumed lunar material of periodotite. In an outer layer ($\sim$ 170 km thick) the temperature rises to 850-1050°K, after which it gradually increases to 1200-1500°K at a depth of $\sim$ 1000 km. From lunar hysteresis curves it has been determined that the global relative magnetic permeability is $\mu/\mu_o = 1.029^{+0.024}_{-0.019}$ for the whole moon. This permeability indicates that the moon responds as a paramagnetic or weakly ferromagnetic sphere; lunar iron abundance is calculated for various compositional models in a companion article (Parkin et al., 1973).

Physics of the Earth and Planetary Interiors, 7 (1973) 251-265
North-Holland Publishing Company, Amsterdam - Printed in The Netherlands

GLOBAL ELECTROMAGNETIC INDUCTION IN THE MOON AND PLANETS

Palmer Dyal and Curtis W. Parkin
Space Science Division, NASA-Ames Research Center, Moffett Field, CA
Department of Physics, University of Santa Clara, Santa Clara, CA

A summary of experiments and analyses concerning electromagnetic induction in the Moon and other extraterrestrial bodies is presented. Magnetic step-transient measurements made on the lunar dark side show the eddy current response to be the dominant induction mode of the Moon. Analysis of the poloidal field decay of the eddy currents has yielded a range of monotonic conductivity profiles for the lunar interior: the conductivity rises from $3 \cdot 10^{-4}$ mho/m at a depth of 170 km to 10^{-2} mho/m at 1000 km depth. The static magnetization field induction has been measured and the whole-Moon relative magnetic permeability has been calculated to be $\mu/\mu_o = 1.01 \pm 0.06$. The remanent magnetic fields, measured at Apollo landing sites, range from 3 to 327 γ. Simultaneous magnetometer and solar wind spectrometer measurements show that the 38-γ remanent field at the Apollo 12 site is compressed to 54 γ by a solar wind pressure increase of $7 \cdot 10^{-8}$ dyn/cm^2. The solar wind confines the induced lunar poloidal field; the field is compressed to the surface on the lunar subsolar side and extends out into a cylindrical cavity on the lunar antisolar side. This solar wind confinement is modeled in the laboratory by a magnetic dipole enclosed in a superconducting lead cylinder; results show that the induced poloidal field geometry is modified in a manner similar to that measured on the Moon. Induction concepts developed for the Moon are extended to estimate the electromagnetic response of other bodies in the solar system.

Proceedings of the Fifth Lunar Science Conference, vol. 3, in press.
(NASA 3/47)

Temperature and electrical conductivity of the lunar interior from magnetic transient measurements in the geomagnetic tail

Palmer Dyal
NASA-Ames Research Center, Moffett Field, California 94035

Curtis W. Parkin
Dept. of Physics, Univ. of Santa Clara, Santa Clara, CA 95053

William D. Daily
Dept. of Physics and Astronomy, Brigham Young Univ., Provo, Utah 84062

Abstract——Magnetometers have been deployed at four Apollo sites on the moon to measure remanent and induced lunar magnetic fields. Global lunar fields due to eddy currents, induced in the lunar interior by magnetic transients, have been analyzed for the first time within the lobes of the geomagnetic tail field. An electrical conductivity profile has been calculated for the moon: the conductivity increases rapidly with depth from 10^{-9} mhos/m at the lunar surface to 10^{-4} mhos/m at 200 km depth, then less rapidly to 2×10^{-2} mhos/m at 1000 km depth. This profile is generally consistent with conductivity results from transient response analysis in the solar wind, using data measured on the lunar nightside. A temperature profile is calculated from conductivity. Using the data of Duba et al. (1974): Temperature rises rapidly with depth to 1100°K at 200 km depth, then less rapidly to 1800°K at 100 km depth. Velocities and thicknesses of the earth's magnetopause and bow shock at the lunar orbit are estimated from simultaneous magnetometer measurements. Average speeds are determined to be about 50 km/sec for the magnetopause and 70 km/sec for the bow shock, although there are large variations in the measurements for any particular boundary crossing. Corresponding measured boundary thicknesses average to about 2300 km for the magnetopause and 1400 km for the bow shock at the position of the lunar orbit.

Proceedings of the Fifth Lunar Science Conference, Vol. 3, in press. (NASA. Vol. 3, No. 48)

Iron abundance and magnetic permeability of the moon

Curtis W. Parkin
Dept. of Physics, Univ. of Santa Clara, Santa Clara, CA 95053

William D. Daily
Dept. of Physics and Astronomy, Brigham Young Univ., Provo, Utah 84062

Palmer Dyal
NASA-Ames Research Center, Moffett Field, California 94035

Abstract—A larger set of simultaneous data from the Apollo 12 lunar surface magnetometer and the Explorer 35 Ames magnetometer are used to construct a whole-moon hysteresis curve, from which a new value of global lunar permeability is determined to be $\mu = 1.012 \pm 0.006$. The corresponding global induced dipole moment is 2.1×10^{18} gauss-cm^3 for typical inducing fields of 10^4 gauss in the lunar environment. From the permeability measurement, lunar free iron abundance is determined to be 2.5±2.0 wt.%. Total iron abundance (sum of iron in the ferromagnetic and paramagnetic states) is calculated for two assumed compositional models of the lunar interior: a free iron/orthopyroxene lunar composition and a free iron/olivine composition. The overall lunar total iron abundance is determined to be 9.0±4.7 wt.%. Other lunar models with a small iron core and with a shallow iron-rich layer are discussed in light of the measured global permeability. Effects on permeability and iron content calculations due to a possible lunar ionosphere are also considered.

Reviews of Geophysics and Space Physics

Magnetism and the Interior Of The Moon

Palmer Dyal
NASA-Ames Research Center, Moffett Field, California 94035

Curtis W. Parkin
Dept. of Physics, Univ. of Santa Clara, Santa Clara, CA 95053

William D. Daily
Dept. of Physics and Astronomy, Brigham Young Univ., Provo, Utah 84062

Abstract——During the time period 1961-1972 eleven magnetometers were sent to the moon. The primary purpose of this paper is to review the results of lunar magnetometer data analysis, with emphasis on the lunar interior. Magnetic fields have been measured on the lunar surface at the Apollo 12, 14, 15, and 16 landing sites. The remanent field values at these sites are respectively 38γ, 103γ (maximum), 3γ, and 327γ (maximum). Simultaneous magnetic field and solar plasma pressure measurements show that the Apollo 12 and 16 remanent fields are compressed during times of high plasma dynamic pressure. Apollo 15 and 16 subsatellite magnetometers have mapped in detail the fields above portions of the lunar surface and have placed an upper limit of 4.4×10^{13} gauss-cm^3 on the global permanent dipole moment. Satellite and surface measurements show strong evidence that the lunar crust is magnetized over much of the lunar globe. Magnetic fields are stronger in highland regions than in mare regions, and stronger on the lunar far side than on the near side. The largest magnetic anomaly measured to date is between the craters Van de Graaff and Aitken on the lunar far side. The origin of the lunar remanent field is not yet satisfactorily understood; several source models are presented. Simultaneous data from the Apollo 12 lunar surface magnetometer and the Explorer 35 Ames magnetometer are used to construct a whole-moon hysteresis curve, from which the global lunar

permeability is determined to be $\mu = 1.012 \pm 0.006$. The corresponding global induced dipole moment is $\sim 2 \times 10^{18}$ gauss-cm^3 for typical inducing fields of 10^{-4} gauss in the lunar environment. From the permeability measurement, lunar free iron abundance is determined to be 2.5 ± 2.0 wt. %. Total iron abundance (sum of iron in the ferromagnetic and paramagnetic states) is calculated for two assumed compositional models of the lunar interior. For a free iron/orthopyroxene lunar composition the total iron content is 12.8 ± 1.0 wt. %; for a free iron/olivine composition, total iron content is 5.5 ± 1.2 wt. %. Other lunar models with a small iron core and with a shallow iron-rich layer are also discussed in light of the measured global permeability. Global eddy current fields, induced by changes in the magnetic field external to the moon, have been analyzed to calculate lunar electrical conductivity profiles using several different analytical techniques. From nightside transient data, ranges of conductivity profiles have been calculated. At a depth of 250 km into the moon, the conductivity ranges between 1×10^{-4} and 2×10^{-3} mhos/meter. Thereafter, conductivity rises with depth and ranges between 2×10^{-3} and 8×10^{-2} mhos/meter at 1000 km depth. Harmonic analyses of dayside data is similar to nightside results except at the greater lunar depths, where harmonic dayside profiles show lower conductivities than do the nightside results. Transient response analysis has recently been applied to data measured in the lobes of the geomagnetic tail, allowing calculation of a conductivity profile which increases with depth from 10^{-9} mhos/meter at the lunar surface to 10^{-4} mhos/meter at 200 km depth, then to 2×10^{-2} mhos/meter at 1000 km depth. This profile is generally consistent with conductivity results from transient response analysis in the solar wind, using data measured on the lunar nightside. A temperature profile is calculated from this conductivity profile, using the data of Duba et al. (1974): temperature rises rapidly with depth to 1100°K at 200 km depth, then less rapidly to 1800°K at 1000 km depth.

Proceedings of the Conference on Cosmochemistry of the Moon and Planets

Lunar Electrical Conductivity, Permeability, and Temperature From Apollo Magnetometer Experiments

Palmer Dyal
NASA-Ames Research Center, Moffett Field, California 94035

Curtis W. Parkin
Dept. of Physics, Univ. of Santa Clara, Santa Clara, CA 95053

William D. Daily
Brigham Young University, Provo, Utah 84602

Abstract—Magnetometers have been deployed at four Apollo sites on the moon to measure remanent and induced lunar magnetic fields. Measurements from this network of instruments have been used to calculate the electrical conductivity, temperature, magnetic permeability, and iron abundance of the lunar interior. The measured lunar remanent fields range from 3 gammas (γ) minimum at the Apollo 15 site to 327 γ maximum at Apollo 16. Simultaneous magnetic field and solar plasma pressure measurements show that the remanent fields at the Apollo 12 and 16 sites interact with, and are compressed by, the solar wind. Remanent fields at Apollo 12 and 16 are increased 16 γ and 32 γ, respectively, by a solar plasma bulk pressure increase of 1.5×10^{-7} dynes/cm^2. Global lunar fields due to eddy currents, induced in the lunar interior by magnetic transients, have been analyzed to calculate an electrical conductivity profile for the moon. From nightside magnetometer data in the solar wind it has been found that deeper than 170 km into the moon the conductivity rises from 3×10^{-4} mhos/m to 10^{-2} mhos/m at 1000 km depth. Recent analysis of data obtained in the geomagnetic tail, in regions free of complicating plasma effects, yields results which are consistent with nightside values. Conductivity profiles have been used to calculate the lunar temperature for an assumed lunar material of olivine. In the outer layer

(~170 km thick) the temperature rises to 1100°C, after which it gradually increases with depth to 1500°C at a depth of ~1000 km. Simultaneous measurements by magnetometers on the lunar surface and in orbit around the moon are used to construct a whole-moon hysteresis curve, from which the global lunar magnetic permeability is determined to be $\mu = 1.012 \pm 0.006$. The corresponding global induced dipole moment is 2×10^{18} gauss-cm^3 for typical inducing fields of 10^{-4} gauss in the lunar environment. Lunar free iron abundance corresponding to the global permeability is determined to be 2.5 ± 2.0 wt. %. Total iron abundance (sum of iron in the ferromagnetic and paramagnetic states) is calculated for two assumed compositional models of the lunar interior. For a free iron/orthopyroxene lunar composition the total iron content is calculated to be 12.8 ± 1.0 wt. %; for a free iron/olivine composition, total iron content is 5.5 ± 1.2 wt. %. Other lunar models with an iron core and with a shallow iron-rich layer are also discussed in light of the measured global lunar permeability. Velocities and thicknesses of the earth's magnetopause and bow shock have been estimated from simultaneous magnetometer measurements. Average speeds are determined to be about 50 km/sec for the magnetopause and 70 km/sec for the bow shock, although there are large variations in the measurement for any particular boundary crossing. Corresponding measured boundary thicknesses average about 2300 km for the magnetopause and 1400 km for the bow shock.

Second General Scientific Assembly, International Assn. of Geomagnetism and Aeronomy, Kyoto, Japan, September 1973.

Lunar Properties From The Apollo Surface Magnetometer Experiments

Curtis W. Parkin
Dept. of Physics, Univ. of Santa Clara, Santa Clara, CA 95053

Palmer Dyal
NASA-Ames Research Center, Moffett Field, California 94035

William D. Daily
NASA-Ames Research Center, Moffett Field, California 94035

Magnetic fields have been measured on the lunar surface at the Apollo 12, 14, 15, and 16 landing sites. The remanent field values at these sites are respectively 38γ, 103γ (maximum), 3γ, and 300γ (maximum). Measurements indicate that the sources of the remanent fields are local rather than global and that on the near-earth hemisphere the highlands possess higher magnetic fields than do the mare regions. Simultaneous magnetic field and solar plasma pressure measurements show that the remanent fields at the Apollo 12 and 16 sites interact with, and are compressed by, the solar wind. Remanent fields at Apollo 12 and 16 sites are increased 16γ and 32γ, respectively, by a solar plasma bulk pressure increase of 1.5×10^{-7} dynes/cm^2. Global lunar fields due to eddy currents, induced in the lunar interior by magnetic step transients in the solar wind, have been analyzed to calculate an electrical conductivity profile for the moon. From nightside magnetometer data it has been found that deeper than 170 km into the moon, the conductivity rises from 3×10^{-4} mhos/m to 10^{-2} mhos/m at 1000 km depth. Analysis of dayside transient are in agreement with the conductivity profile determined from nightside data. The conductivity profile is used to calculate the temperature for an assumed lunar material of peridotite. In an outer layer (~170 km thick) the temperature rises to 850-1050°K, after which it gradually increases to 1200-1500°K at

a depth of ~1000km. Whole-moon hysteresis curves are plotted using Apollo 12 and 15 lunar surface magnetometer data with simultaneous lunar orbiting Explorer 35 data. From these curves a global relative permeability $\mu/\mu_o = 1.029 \, ^{+0.024}_{-0.019}$ is calculated. This result implies that the moon is not composed entirely of paramagnetic material, but that ferromagnetic material such as free iron exists in sufficient amounts to dominate the bulk lunar magnetic susceptibility. From the magnetic data the ferromagnetic free iron abundance is calculated. Then for assumed compositional models of the moon the additional paramagnetic iron is determined, yielding total lunar iron content. The calculated abundances are as follows: ferromagnetic free iron, 5 ± 4 wt. %; total iron in the moon, 9 ± 4 wt. %.

Second General Scientific Assembly, International Assn. of Geomagnetism and Aeronomy, Kyoto, Japan, September, 1973.
Abstract of IAGA/IUGG Conference, September 9-21, 1973

Lunar Electrical Conductivity Profile Analysis

A. F. Kuckes
Cornell University, Ithaca, N.Y. 14850, U.S.A.

S. V. Beckwith
Cornell University, Ithaca, N.Y. 14850, U.S.A.

William D. Daily
NASA-Ames Research Center, Moffett Field, California 94035

Palmer Dyal
NASA-Ames Research Center, Moffett Field, California 94035

Curtis W. Parkin
Dept. of Physics, Univ. of Santa Clara, Santa Clara, CA 95053

The analysis of magnetic fluctuations on the lunar surface and their correlation with the fluctuations nearby in space has been extended to lower frequencies to set limits on the conductivity and temperature of the lunar core. Simple Fourier analysis of transients, particularly those with a period of more than an hour has been performed. Attention has been directed to examining the self consistency of daytime and nighttime observations and the effects of the solar wind conductivity, diamagnetism and shadow behind the moon. The conductivity and temperature implied by these results on the core region inside about 2/3 of the lunar radius will be discussed.

The Geological Society of America, Annual conference, Dallas, Nov. 1973.

Lunar Properties From The Apollo Surface Magnetometer Experiments

Palmer Dyal
Space Science Division, NASA-Ames Research Center, Moffett Field, CA

Curtis W. Parkin
Department of Physics, University of Santa Clara, Santa Clara, CA

William D. Daily
Space Science Division, NASA-Ames Research Center, Moffett Field, CA

Magnetometers have been deployed at four Apollo sites on the moon to measure remanent and induced lunar magnetic fields. Measurements from this network of instruments have been used to calculate the electrical conductivity, temperature, magnetic permeability, and iron abundance of the lunar interior. The remanent fields range from 3γ as minimum at the Apollo 15 site to 327γ maximum at Apollo 16. The field sources are local rather than global and on the near-earth hemisphere the highlands possess higher magnetic fields than do the mare regions.

Induced lunar fields, due to eddy currents in the interior, are global in extent and have been analyzed to calculate an electrical conductivity profile for the moon: The conductivity rises from 3×10^{-4} mhos/m to 10^{-2} mhos/m at 1000 km depth. The conductivity profile is used to calculate the temperature for assumed material models of the lunar interior. Whole-moon hysteresis curves are plotted using magnetometer data from two surface sites with simultaneous lunar orbiting Explorer 35 data. From these curves, a global relative permeability of $1.029^{+0.024}_{-0.019}$ is calculated. This result implies that the moon is not composed entirely of paramagnetic material, but that ferromagnetic material such as free iron exists in sufficient amounts to dominate the bulk lunar magnetic susceptibility. From the magnetic data, lunar iron abundances are calculated: ferromagnetic free iron, 5 ± 4 weight percent: total iron in the moon, 9 ± 4 weight percent.

Lunar Science V, Fifth Lunar Science Conference, March 1974.

Lunar Iron Abundance From Magnetometer Measurements

Curtis W. Parkin
Dept. of Physics, Univ. of Santa Clara, Santa Clara, CA 95053

William D. Daily
Brigham Young University, Provo, Utah 84602

Palmer Dyal
NASA-Ames Research Center, Moffett Field, California 94035

Simultaneous measurements by magnetometers on the lunar surface and in orbit around the moon are used to construct a whole-moon hysteresis curve, from which the global lunar magnetic permeability is determined to be $\mu = 1.012 \pm 0.006$. The corresponding global induced dipole moment is 2×10^{18} gauss-cm^3 for typical inducing fields of 10^{-4} Oe in the lunar environment. Lunar free iron abundance corresponding to the global permeability is determined to be 2.5 ± 2.0 wt %; the value within this range is dependent upon location of the Curie isotherm in the lunar interior. Total iron abundance (sum of iron in the ferromagnetic and paramagnetic states) is calculated for two assumed compositional models of the lunar interior. For a free iron/orthopyroxene lunar composition the total iron content is 12.8 ± 1.0 wt %; for a free iron/olivine composition, total iron content is 5.5 ± 1.2 wt %. Other lunar models with an iron core and with a shallow iron-rich layer are also discussed in light of the measured global lunar permeability.

Lunar Science V, Fifth Lunar Science Conference, March 1974

Global Lunar Properties From Magnetometer Measurements

Palmer Dyal
NASA-Ames Research Center, Moffett Field, California 94035

Curtis W. Parkin
Dept. of Physics, Univ. of Santa Clara, Santa Clara, CA 95053

William D. Daily
Brigham Young University, Provo, Utah 84602

Magnetometers have been deployed at four Apollo sites on the moon to measure remanent and induced lunar magnetic fields. Measurements from this network of instruments have been used to calculate the electrical conductivity, temperature, magnetic permeability, and iron abundance of the lunar interior. Global lunar fields due to eddy currents, induced in the lunar interior by magnetic transients, have been analyzed to calculate an electrical conductivity profile for the moon. From nightside magnetometer data in the solar wind it has been found that deeper than 170 km into the moon the conductivity rises from 3×10^{-4} mhos/m to 10^{-2} mhos/m at 1000 km depth. Recent analysis of data obtained in the geomagnetic tail, in regions free of complicating plasma effects, yields results which are slightly lower than nightside values. Conductivity profiles calculated from data obtained in the geotail region will be presented. The conductivity profile is used to calculate the temperature for an assumed lunar material of olivine. In an outer layer ($\sim$170 km thick) the temperature rises to 1100 ^{o}C, after which it gradually increases to 1500 ^{o}C at a depth of $\sim$1000 km. Whole-moon hysteresis curves are plotted using Apollo 12 lunar surface magnetometer data with simultaneous lunar orbiting Explorer 35 data. From these curves a new global relative permeability $\mu/\mu_o = 1.012 \pm 0.006$ is calculated.

From the magnetic data the free iron abundance is calculated to be 2.5 wt %. The remanent fields range from 3γ as minimum at the Apollo 15 site to 327γ maximum at Apollo 16. Simultaneous magnetic field and solar plasma pressure measurements show that the remanent fields at the Apollo 12 and 16 sites interact with, and are compressed by, the solar wind. Remanent fields at Apollo 12 and 16 sites are increased 16γ and 32γ, respectively, by a solar plasma bulk pressure increase of 1.5×10^{-7} dynes/cm^2.

Trans. Amer. Geophys. Union (EOS), 55, p. 331, April 1974

Temperature Profile of the Lunar Interior

A. F. Kuckes
Dept. of Applied Physics, Cornell University, Ithaca, N.Y. 14850

William D. Daily
Dept. of Physics and Astronomy, Brigham Young Univ., Provo, Utah 84601

Palmer Dyal
NASA-Ames Research Center, Moffett Field, California 90053

Curtis W. Parkin
Dept. of Physics, Univ. of Santa Clara, Santa Clara, CA 95053

The experimentally deduced lunar transfer function for magnetic fluctuations is compared to that computed from several thermal profiles of the lunar interior. A compositionally uniform moon whose electrical conductivity is that of a semi-conductor, i.e., $\sigma = \sigma_o e^{-\epsilon/kT}$ was assumed. Since the detailed composition and electrical conductivity are not well known, the quantities σ and ϵ were kept arbitrary. With these suppositions the shape of the experimentally observed transfer function strongly implies a lunar lithosphere about 200 km thick where heat transfer is dominated by conduction and a thermally uniform core where heat transport is dominated by slow convection. These conclusions are numerically consistent with the laboratory observations of Duba, Heard and Schock, the experimentally observed heat flux of Langseth, Clark, Chute, Keihm, and Wechsler and the general considerations of Turcotte, Hsui, Torrance and Oxburgh. Our results are in serious variance with lunar models requiring a significant thermal gradient to depths below 300 km. The lunar transfer function between 3×10^{-5} and 5×10^{-3} Hz was obtained by Fourier analyzing simultaneous magnetic transients recorded by Apollo 12 and Explorer 35. Lunar daytime and night time data yield consistent results. Small but significant corrections must be made to take into account the diamagnetism of the solar wind.

Trans. Amer. Geophys. Union (EOS), 55, p. 390, April 1974

Magnetopause Velocity and Thickness Determined from a Network of Apollo Magnetometers

William D. Daily
Dept. of Physics and Astronomy, Brigham Young Univ., Provo, Utah 84601

Palmer Dyal
NASA-Ames Research Center, Moffett Field, California 90053

Curtis W. Parkin
Dept. of Physics, Univ. of Santa Clara, Santa Clara, CA 95053

The velocity and thickness of the magnetopause at 60 R_E have been measured using a network of magnetometers on the lunar surface and in orbit around the moon. Multiple magnetopause crossings from five lunar orbits through the geomagnetic tail have been analyzed. Velocities have been calculated by measuring the time delays of boundary crossings from simultaneous data. Typical velocities range from 10 km/sec to 100 km/sec, with occasional higher velocities observed. Estimates for the thickness of the magnetopause current layer responsible for magnetic field changes through the boundary range from 1000 km to 6000 km. Results will also be reported from a similar study of the bow shock and neutral sheet.

Annual Progress Report

Hans R. Aggarwal

Research during February 1974 to August 1974 has continued in association with Dr. Verne R. Oberbeck of the NASA-Ames Research Center. Progress was made towards achieving the objectives, which are to carry out theoretical studies to further our understanding of crater formation mechanisms on planetary surfaces and to perform analyses to interpret their geologic history. A brief description of the tasks completed during this period is as follows:

1. Developed a code and a program to digitize the crater data and to reformat the Calma 303 tape to run on IBM 360/67 system.
2. Accumulated and reduced the data of Mariner 9 photographs. Developed a method to calculate the co-ordinates (latitude & longitude) of a martian feature in terms of the co-ordinates of its neighboring points.
3. Calculated circularity index of certain lunar craters.

Further work in continuation of the above tasks is under progress. Mr. Leonard Trammiel, student Department of Physics of the University of Santa Clara, assisted in the reduction of the martian data.

The paper on Roche Limit submitted for publication previously appeared in the July issue of the Astrophysical Journal. A copy of its abstract is enclosed.

THE ASTROPHYSICAL JOURNAL, 191:577-588, 1974 July 15

ROCHE LIMIT OF A SOLID BODY

H.R. AGGARWAL* AND V.R. OBERBECK
Ames Research Center, NASA, Moffett Field, California
Received 1973 September 24; revised 1974 February 22

ABSTRACT

Tidal fission of both impacting and orbiting linear elastic solid bodies based on Kelvin's theory of Earth tides is considered. It is shown that there can be more than one mutually exclusive mode of fracture-the particular mode in which a body fractures depending on its size and strength. The analysis gives a vivid picture of the propagation of the fracture with a decreasing distance from the planet. Expressions for the initiation and completion of fracture are obtained which are displayed graphically for a rigid body. The effect of elasticity on the breakup altitude is discussed. For orbiting solid bodies, the study gives the upper limit of the break-up altitude as 0.38R (where R is the radius of planet), which is much less than the value 1.44R used for such bodies in the past. The results presented include a previously given theory by Sekiguchi as a part. For the special case of a liquid body, comparison is made with Roche's calculation and the difference explained.